

Comparison of Microstructure and Mechanical Properties of RPVs used in Korea Standard Nuclear Power Plant OPR1000 and APR1400

Seokmin Hong^a, Cholong Lee^b, Ki-Deuk Min^a, Min-Chul Kim^{a*}, Bong-Sang Lee^a

^aNuclear Materials Research Division, Korea Atomic Energy Research Institute, Deokjin dong, Daejeon, Korea.

^bQuantum Energy Chemical Engineering, University of Science & Technology, Daejeon, Korea.

*Corresponding author: mckim@kaeri.re.kr

1. Introduction

Safety issues becomes most important in nuclear power plant operation. Reactor pressure vessels (RPVs), which comprise the major component in several classes of nuclear reactors, are subject to irradiation embrittlement due to high-energy neutron exposure. Commercial RPVs are made from SA508 Gr.3, Mn-Mo-Ni low alloy steel, which possesses high strength and excellent toughness to prevent unexpected failure during both normal operation and unanticipated accident conditions [1-3]. The microstructure of SA508 Gr.3 alloy is known as bainitic microstructure [4,5]. Recent studies of the microstructure of SA508 Gr.3 reported that macrosegregation occurred in the huge steel ingots, which led to spatial variations in the microstructure. The typical microstructure in solute-enriched regions was composed of Widmanstatten ferrite, lower bainite, and martensite-austenite islands, whereas the typical microstructure in solute-depleted regions was composed of allotriomorphic ferrite, which can lead to deterioration of toughness [6,7].

In order to increase generation capacity, APR1400 have increased the size. Size of RPV in APR1400 also increased [8,9]. Detailed feature and spec are described in figure 1 and table 1. Larger ingot size could cause microstructural inhomogeneity problems. To assure the improved safety of APR1400, properties of RPV in APR1400 need to be checked. Thus, in this study, variations of microstructure and mechanical properties of RPV in APR1400 were investigated and compared with those in OPR1000 [10-12].

Table 1. Spec of OPR1000 and APR1400 RPV

| 부품 | 항목 | OPR1000 | APR1400 |
|-------------|----|-----------------|-----------------|
| 원자로 압력용기 | 내경 | 414 cm | 462.92 cm |
| | 두께 | 20.5 cm Min. | 23.0 cm Min. |
| | 높이 | 1,464.2 cm | 1,463 cm |
| | 무게 | 436 ton | 533 ton |

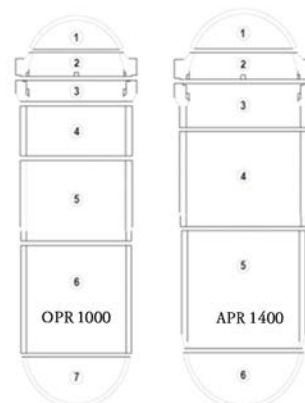


Figure 1. Schematic Image of OPR1000 and APR1400 RPV

2. Experiments and Results

2.1 Microstructure

The tested material was an archive of SA 508 Gr.3 Cl.1 heavy-section Mn-Mo-Ni low alloy steel, a domestic RPV steel used in OPR1000 and APR1400. The OPR1000 and APR1400 RPV was manufactured by vacuum carbon deoxidation (VCD) and VCD+Si killed+Al method, respectively. Test specimens were sampled from the inner surface, 1/4 thickness, the center, 3/4 thickness, and the outer surface at intervals of 1/4 thickness of the RPV toward the center from the inner surface. For convenience, these regions are referred to as 0T (inner surface), 1/4T, 1/2T (center), 3/4T, and 1T (outer surface).

The chemical compositions were measured using emission spectrochemical analysis, and the results are shown in Table 2. The chemical analysis revealed that the contents of P and S, elements that can lead to deterioration of mechanical properties [13], were very low. The content of Cu, a deteriorative element that can cause irradiation embrittlement [14-15], was less than 0.03 wt%, which satisfied the specification for 60-year operation [16].

The longitudinal-short transverse (L-S) planes of the steel were polished and etched with a 2% nital solution, and the microstructures were observed using an optical

microscope (OM; model, eclipse MA 200, Nikon, Japan). OM images of RPV are shown in Figure 2 and 3 respectively, and various microstructural constituents are marked in the micrographs.

In the case of OPR1000 RPV, microstructure was fully composed of bainite. At the surface (0T, 1T), the microstructure mainly consisted lower bainite and fine lath upper bainite (B). At the 1/4T and 3/4T location, coarse lath upper bainite (UB) began to form, and B decreased. The volume fraction of UB increased moving toward the center from the surfaces. At 1/2T microstructure consisted UB.

In the case of APR1400 RPV, microstructure was different to OPR1000 RPV. At the surface (0T, 1T), the microstructure mainly consisted coarse lath upper bainite (UB). At the 1/4T and 3/4T location, quasi-polygonal ferrite began to form. The volume fraction of polygonal ferrite increase moving toward the center from the surface. Compared to the OPR1000 RPV, grain size of APR1400 is smaller.

Table 2. Chemical compositions of RPV in OPR1000 and APR1400 [12]

| Samples | Positions | C | Mn | Mo | Ni | Cr | Si | Cu | P | S |
|--------------------|-----------|-------------|---------------|---------------|---------------|-------------|-------------|-------------|--------------|--------------|
| SA508 Gr.3 CL.1 | 1/4T | 0.25 max | 1.20- 1.50 | 0.45- 0.60 | 0.40- 1.00 | Max 0.25 | 0.40 max | 0.20 max | 0.025 max | 0.025 max |
| ORV | 0T | 0.22 | 1.39 | 0.47 | 0.81 | 0.15 | 0.045 | 0.03 | 0.003 | - |
| | 1/4T | 0.25 | 1.44 | 0.51 | 0.84 | 0.16 | 0.048 | 0.03 | 0.003 | - |
| | 1/2T | 0.23 | 1.41 | 0.49 | 0.82 | 0.16 | 0.046 | 0.03 | 0.003 | - |
| | 3/4T | 0.22 | 1.40 | 0.48 | 0.82 | 0.16 | 0.047 | 0.03 | 0.003 | - |
| | 1T | 0.22 | 1.41 | 0.50 | 0.82 | 0.16 | 0.047 | 0.03 | 0.003 | - |
| ARV | 0T | 0.22 | 1.13 | 0.49 | 0.86 | 0.19 | 0.21 | 0.021 | 0.004 | - |
| | 1/4T | 0.21 | 1.12 | 0.48 | 0.85 | 0.19 | 0.21 | 0.022 | 0.004 | - |
| | 1/2T | 0.20 | 1.14 | 0.50 | 0.86 | 0.20 | 0.21 | 0.024 | 0.004 | - |
| | 3/4T | 0.20 | 1.15 | 0.49 | 0.87 | 0.20 | 0.21 | 0.021 | 0.004 | - |
| | 1T | 0.21 | 1.15 | 0.50 | 0.86 | 0.20 | 0.22 | 0.021 | 0.004 | - |

:- non-detect, S detection limit: 0.002

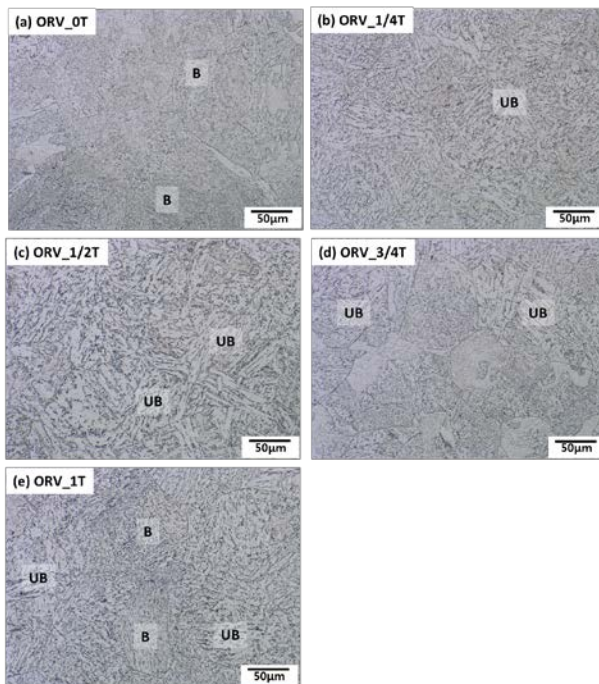


Figure 2. OM images of OPR1000 RPV along the depth positions [12]

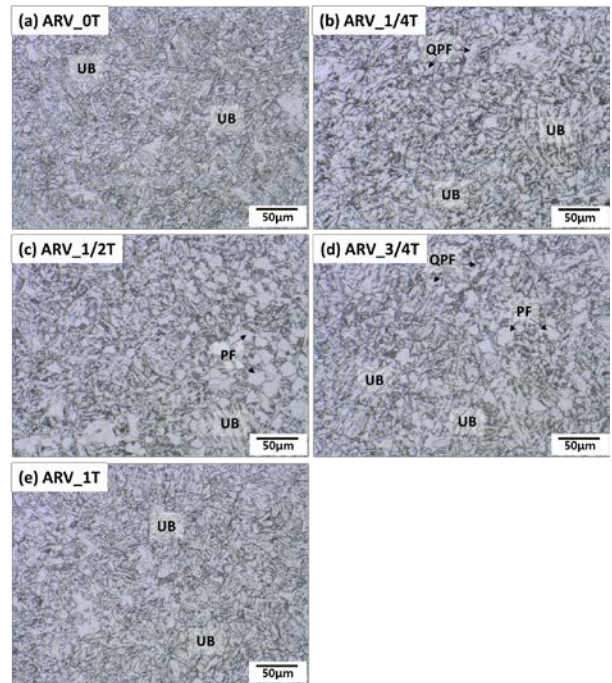


Figure 3. OM images of APR1400 RPV along the depth positions [12]

2.2 Mechanical Properties

Round bar-type tensile specimens (gauge length 25 mm, diameter 6.25 mm) were prepared in the transverse direction and were tested at room temperature using a universal testing machine (model MTS 810, MTS, USA) with a 10-ton capacity under a strain rate of 5.2×10^{-4} , according to ASTM E8/E8M [14]. The 0.2% offset stress method was used to determine the yield strength from the engineering stress-strain curves. Tensile properties were listed in table 2.

Both RPV steels shows highest yield strength and tensile strength at the inner surface (0T). Toward the center, strength tend to decrease. In case of APR1400 RPV, tensile properties are symmetric along the center position. However OPR1000 RPV tensile properties at outer position (3/4T, 1T) are worse than inner position (1/4T, 0T). Compared to OPR1000 RPV, APR1400 RPV shows higher strength.

Table 3. Tensile Properties of OPR1000 RPV and APR1400 RPV along the depth position [12]

| Samples | Positions | Tensile Properties | | |
|--------------------|-----------|--------------------|----------|----------|
| | | YS (MPa) | TS (MPa) | El.(%) |
| OPR1000 RPV | 0T | 422±6 | 580±5 | 28.4±0.8 |
| | 1/4T | 408±1 | 566±2 | 27±1.0 |
| | 1/2T | 405±3 | 558±4 | 28.1±0.4 |
| | 3/4T | 397±1 | 547±1 | 25.1±0.2 |
| | 1T | 401±1 | 549±2 | 24.1±0.8 |
| APR1400 RPV | 0T | 466±1 | 622±1 | 26.7±0.5 |
| | 1/4T | 436±2 | 586±1 | 29.8±1.0 |
| | 1/2T | 408±1 | 556±2 | 29.2±0.1 |
| | 3/4T | 435±1 | 584±1 | 28.9±0.7 |
| | 1T | 443±2 | 579±1 | 28.1±0.3 |
| ASME SA508 Gr.3 | 1/4T | 345 min. | 550-725 | 18 min. |

Charpy impact tests were performed on standard Charpy V-notch specimens (standard size; 10 mm × 10 mm × 55 mm, transverse-longitudinal (T-L) orientation) using an impact test machine (model: SI-1D3, SATEC, USA) with a 406 J capacity in the temperature range from -100 °C to 300 °C, according to ASTM E23 [18]. To reduce errors in data interpretation, a regression analysis for absorbed impact energy vs. test temperature was performed using a hyperbolic tangent curve-fitting method [19]. The regression analysis data were used to determine the upper shelf energy (USE), index temperature (T_{41J}) [20], and energy transition temperature (ETT). The ETT corresponds to the average value of the USE and the lower shelf energy (LSE), and the index temperature (T_{41J}) is determined at the absorbed energy of Charpy test corresponding to 41 J.

Charpy impact properties are listed in table 4. Both RPV steels shows lowest ETT and index temperature at the inner surface (0T). In the case of OPR1000 RPV, impact properties at 1/4T were worst. In the case of APR1400 RPV, ETT and index temperature tend to increase toward the center and they are symmetric along the center position. Compared to OPR1000 RPV, APR1400 RPV shows lower ETT and index temperature.

Table 4. Charpy impact properties of OPR1000 RPV and APR1400 RPV along the depth position [12]

| Samples | Positions | Charpy Impact Properties | | |
|-------------|-----------|--------------------------|---------|----------------|
| | | USE (J) | ETT(°C) | T_{41J} (°C) |
| OPR1000 RPV | 0T | 328 | -6.8 | -66.9 |
| | 1/4T | 258 | 10.2 | -14.4 |
| | 1/2T | 291 | 4.6 | -25.9 |
| | 3/4T | 297 | -6.8 | -40.3 |
| | 1T | 303 | -3.6 | -30.5 |
| APR1400 RPV | 0T | 287 | -29 | -76 |
| | 1/4T | 302 | -6 | -53 |
| | 1/2T | 332 | -2 | -40 |
| | 3/4T | 283 | -14 | -45 |
| | 1T | 318 | -25 | -74 |

3. Discussion

Microstructures of OPR1000 and APR1000 were mainly composed of bainite, but detail microstructure was different. OPR1000 RPV was fully composed of bainite structure. At the surface fine lath upper bainite and lower bainite were mainly observed. Toward the center, bainite lath coarsened and coarse lath upper bainite formed. In the APR1400 RPV, coarse lath upper bainite was formed at surface. Toward the center, bainite lath coarsened and polygonal ferrite was formed.

Those microstructure variation along the thickness was caused by cooling rate difference. Because of material's thick thickness, cooling rate difference occurred during heat treatment (austenitizing-water quenching). It resulted in formation of fine lath bainite at the surface and coarse lath bainite at the center. Size of APR1400 was larger than OPR1000. Cooling rate of the APR1400 might be slower than the OPR1000. Therefore APR1400 have coarse lath bainite structure at the surface and polygonal ferrite at the center. But APR1400 was fabricated the VCD+Si+Al method. The addition of Al resulted in the formation of AlN precipitates at high temperature, and suppressed the grain growth of austenite during steel making process. Thus grain size of APR1400 was smaller than OPR1000. In the emission spectrochemical analysis and microstructure analysis, evidences for macro-segregation were not observed.

Both RPV materials shows high strength and low ETT at the surface because surface have fine bainite microstructure. The APR1400 RPV shows higher strength and lower ETT than OPR1000 RPV because it have smaller grain size.

4. Conclusions

1. The macro-segregation problems were not observed in the OPR1000 and APR1400 RPV.
2. Cooling rate difference caused microstructure variation along thickness. Fine lath bainite structure was formed at surface and coarse lath bainite was formed toward the center. In the APR1400 RPV polygonal ferrite structure was observed at the center.
3. APR1400 showed fine grain size because it was fabricated by VCD+Si+Al method. The addition of Al resulted in the formation of AlN precipitates at high temperature, and suppressed the grain growth of austenite during steel making process.
4. APR1400 showed higher strength and lower ETT and index temperature because of smaller grain size.

REFERENCES

- [1] S.G. Druce and B.C. Edward, Nucl. Eng., Vol. 19, p. 347, 1980.
- [2] K. Suzuki, J. Nucl. Mater., Vol. 108-109, p. 443, 1982.
- [3] Code of Federal Regulations, 10 CFR Part 50.61, US Nuclear Regulatory Commission, 2015.
- [4] P. Bernabei, L. Callegari, M. Scepti, and T. Salinetti, Steel Forgings (eds. E.G. Nisbett and A.S. Melilli), p.

- 275, American Society for Testing and Materials, Philadelphia, PA, 1986.
- [5] J.H. Hong, B.J. Lee, and H.D. Kim, *Met. Mater. Trans. A*, Vol. 29A, p. 1441, 1998.
- [6] H. Pous-Romero and H.K.D.H. Bhadeshia, *Metall. Mater. Trans. A*, Vol. 45A, p. 4897, 2014.
- [7] E.J. Pickering and H.K.D.H. Bhadeshia, *Metall. Mater. Trans. A*, Vol. 45A, p. 2983, 2014.
- [8] Kepco-enc., ORP 1000, <http://www.kepco-enc.com/portal/contents.do?key=1239>, 2017.
- [9] Kepco-enc., APR1400, <http://www.kepco-enc.com/portal/contents.do?key=1240>, 2017.
- [10] S. Hong, J. Song, M.C. Kim, K.J. Choi, and B.S. Lee, *Met. Mater. Int.*, Vol. 22, p. 196, 2016.
- [11] J. Song, M.C. Kim, S. Hong, and B.S. Lee, *Korean J. Met. Mater.*, Vol. 53, p. 700, 2015.
- [12] S. Hong, C.L. Lee, M.C. Kim, and B.S. Lee, *J. Met. Mater.*, In Progress, 2017.
- [13] K.J. Harrelson, S.H. Rou, and R.C. Wilcox, *J. Nucl. Mater.*, Vol. 141-143, p. 508, 1986.
- [14] L. Debarberis, F. Sevini, B. Acosta, A. Kryukov, Y. Nikolaev, A.D. Amaev, and M. Valo, *Int. J. Pressure Vessel Piping*, Vol. 79, p. 637, 2002.
- [15] A. Ballesteros, R. Ahlstrand, C. Bruynooghe, U. von Estorff, and L. Debarberis, *Nucl. Eng. Des.*, Vol. 243, p. 63, 2012.
- [16] J.H. Hong, *Nuclear Materials*, 1st ed., pp. 305-323, HANS House, Seoul, 2012.
- [17] ASTM E8/E8M-15, *Annual Book of ASTM Standards*, ASTM, West Conshohocken, PA, 2015.
- [18] ASTM Standard E23-12c, *Annual Book of ASTM Standards*, ASTM, West Conshohocken, PA, 2012.
- [19] W. Oldfield, *ASTM Standardization News* 3, 24, 1975.
- [20] *Regulatory Guide 1.99, Rev.2*, US Nuclear Regulatory Commission, 1988.